DR7dA, a Novel Antioxidant Peptide Analog, Demonstrates Antifibrotic Activity in Pulmonary Fibrosis *In Vivo* and *In Vitro*[S]

Lu Cheng, Dan Wang, Bochuan Deng, Jieru Li, Jiao Zhang, Xiaomin Guo, Tiantian Yan, Xin Yue, Yingying An, Bangzhi Zhang, and Junqiu Xie

Key Laboratory of Preclinical Study for New Drugs of Gansu Province, School of Basic Medical Sciences & Research Unit of Peptide Science, Chinese Academy of Medical Science, 2019RU066 (L.C., D.W., B.D., J.L., J.Z., X.G., T.Y., X.Y., Y.A., B.Z., J.X.) and School of Life Sciences (L.C., D.W.), Lanzhou University, Lanzhou, China

ABSTRACT

Pulmonary fibrosis (PF), which is characterized by enhanced extracellular matrix (ECM) deposition, is an interstitial lung disease that lacks an ideal clinical treatment strategy. It has an extremely poor prognosis, with an average survival of 3–5 years after diagnosis. Our previous studies have shown that the antioxidant peptide DR8 (DHNNPQIR-NH$_2$), which is extracted and purified from rapeseed, can alleviate PF and renal fibrosis. However, natural peptides are easily degraded by proteases *in vivo*, which limits their potency. We have since synthesized a series of DR8 analogs based on amino acid scanning substitution. DR7dA [DHNNPQ (D-alanine) R-NH$_2$] is an analog of DR8 in which L-isoleucine (L-Ile) is replaced with D-alanine (D-Ala), and its half-life is better than that of DR8. In the current study, we verified that DR7dA ameliorated tumor growth factor (TGF)-β1-induced fibrogenesis and bleomycin-induced PF. The results indicated that DR7dA reduced the protein and mRNA levels of TGF-β1 target genes in TGF-β1–induced models. Surprisingly, DR7dA blocked fibrosis in a lower concentration range than DR8 in cells. In addition, DR7dA ameliorated tissue pathologic changes and ECM accumulation in mice. BLM caused severe oxidative damage, but administration of DR7dA reduced oxidative stress and restored antioxidant defense. Mechanistic studies suggested that DR7dA inhibits ERK, P38, and JNK phosphorylation *in vivo* and *in vitro*. All results indicated that DR7dA attenuated PF by inhibiting ECM deposition and oxidative stress via blockade of the mitogen-activated protein kinase (MAPK) pathway. Hence, compared with its parent peptide, DR7dA has higher druggability and could be a candidate compound for PF treatment in the future.

SIGNIFICANCE STATEMENT

In order to improve druggability of DR8, we investigated the structure–activity relationship of it and replaced the L-isoleucine with D-alanine. We found that the stability and antifibrotic activity of DR7dA were significantly improved than DR8, as well as DR7dA significantly attenuated tumor growth factor (TGF)-β1-induced fibrogenesis and ameliorated bleomycin-induced fibrosis by inhibiting extracellular matrix deposition and oxidative stress via blockade of the MAPK pathway, suggesting DR7dA may be a promising candidate compound for the treatment of PF.

Introduction

Pulmonary fibrosis (PF) is a chronic disease characterized by interstitial inflammation and fibrosis. In PF, abnormal fibroblast and myofibroblast differentiation results in α-smooth muscle actin (α-SMA) expression and extracellular matrix (ECM) deposition. Increased ECM results in loss of lung compliance and damage to alveolar structure, eventually leading to respiratory failure and death. In recent years, the incidence and mortality of PF have been increasing gradually; thus, PF is an important human health issue (Distler et al., 2019; Thannickal et al., 2004; Wynn, 2008). At present, pirfenidone and nintedanib are approved for clinical use in delaying the progression of PF, but they cannot reverse the fibrosis process. In addition, pirfenidone can cause some side effects, such as photosensitivity, rashes, and gastrointestinal discomfort (Galli et al., 2017). Lung transplantation is the most effective way to prolong patient survival. However, the widespread application of lung transplantation is limited by the high difficulty and

ABBREVIATIONS: BLM, bleomycin; CAT, catalase; DCFH-DA, 2',7'-dichlorodihydrofluorescein diacetate; ECM, extracellular matrix; EMT, epithelial-mesenchymal transition; FBS, fetal bovine serum; GAPDH, glyceraldehyde-3-phosphate dehydrogenase; GSH, glutathione; HRP, horseradish peroxidase; IL, interleukin; MAPK, mitogen-activated protein kinase; MDA, malondialdehyde; MMP2, matrix metalloproteinase 2; MTT, 3-(4,5-Dimethylthiazol-2-yl)-2,5-diphenyltetrazolium bromide; NAC, N-acetyl-L-cysteine; NOX, NADPH oxidase; OS, oxidative stress; PF, pulmonary fibrosis; ROS, reactive oxygen species; RP-HPLC, reverse-phase high performance liquid chromatography; α-SMA, α-smooth muscle actin; SOD, superoxide dismutase; TGF-β1, transforming growth factor (TGF)-β1; TNF, tumor necrosis factor.

cost of surgery, the lack of lung resources, and the occurrence of immune rejection (George et al., 2019). Therefore, it is necessary to find an effective medicine to alleviate PF.

Transforming growth factor (TGF)-β1 is a main profibrotic cytokine involved in the inflammatory response, oxidative stress (OS), myofibroblast differentiation, and ECM deposition (Saito et al., 2018). OS involves an imbalance of antioxidant and prooxidant processes, including reactive oxygen species (ROS) production and/or antioxidant defense impairment. OS is implicated as an important factor in the pathogenesis of PF, which involves alveolar epithelial cell injury and apoptosis and fibroblast proliferation and differentiation (Kliment and Oury, 2010). In view of the role of OS in the occurrence and development of PF, we believe that antioxidants may play an antifibrotic role in PF. In our previous studies, we reported that the rapeseed (*Brassica campestris* L.)-derived antioxidant peptide DR8 (DHNNPQIR-NH$_2$) can block the progression of PF and renal fibrosis (Deng et al., 2020; Wang et al., 2019).

Peptide drugs typically have the advantages of high efficiency and low toxicity, so research on new peptide drugs has increased in recent years. However, natural active peptides are easily degraded by endogenous proteases, and their poor stability and short half-lives (t$_{1/2}$ values) have limited their applications in medicine (Fosgerau and Hoffmann, 2015). Chemical modification strategies, including the introduction of nonnatural amino acids, cyclization, skeleton modification, and side chain modification, are commonly used to improve the stability of natural peptides (Erak et al., 2018; Werle and Bernkop-Schnurch, 2006). Among these approaches, the introduction of D-type amino acids into the peptide sequence is the most common, simple, and effective strategy to prevent degradation. In our previous studies on alanine (Ala) and D-amino acid scanning analogs of DR8, we found that the activity was retained after replacement of isoleucine (Ile) with Ala but lost after replacement with D-Ile (Wang et al., 2021). Since replacing L-amino acids with nonnatural D-amino acids can improve stability and since D-Ala is readily available, we chose to replace the Ile of DR8 with D-Ala. To investigate whether the modified peptide has greater stability in serum and retains the antifibrotic activity of the parent peptide, a TGF-β1–induced cell model and a bleomycin (BLM)-induced mouse model were used to validate the new analog in the current study.

Materials and Methods

Peptide Synthesis. DR7dA was prepared with the 9-fluorenylmethyloxycarbonyl solid-phase method (Blanco-Canosa and Dawson, 2008; Chandrudu et al., 2013). The peptide was purified and verified by reverse-phase high performance liquid chromatography (RP-HPLC) (Waters Corporation; Milford, MA) to >95% homogeneity with acetonitrile (5–95% in 30 min). Mass spectrometry (MaXis 4G; Bruker) was used to confirm the chemical identity of the peptide.

Serum Stability Study. Serum stability has been widely used in many reports (Hong et al., 1999; Jenssen and Aspmo, 2008; Kim et al., 2010; Noto et al., 2008), and we verified this assay. This experiment was performed as described in a previous study (Wang et al., 2021). The peptide (56 μl of 10 mM) was added to normal mouse serum (224 μl) and incubated at 37°C. An aliquot of 40 μl was taken at 0, 15, 30, 60, 120 and 240 min, and an equal volume of acetonitrile was added to precipitate serum proteins. The mixture was incubated on ice (10 min). After centrifugation (13,000 × g, 15 min), the

supernatant was stored at −80°C. Samples (20 μl) were analyzed by RP-HPLC to determine the t$_{1/2}$. The enzymatic hydrolysis processes of the peptide conformed to the first-order kinetic equation: $A_t = A_0 e^{-Kt}$, when $A_t/A_0 = 0.5$ and $t_{1/2} = \ln 2/K$.

Cell Culture and Treatment. A549 cells were grown in 1640 (Gibco; Carlsbad, CA), and NIH3T3 were grown in Dulbecco's modified Eagle's medium (Gibco) with 10% fetal bovine serum (FBS, Biological Industries, Beit-Haemek, Israel) at 37°C in 5% CO$_2$. Through the retrieval of relevant literature, it is not difficult to find that 1–10 ng/ml TGF-β1 was used to induce cell models, and many results show that 5 ng/ml TGF-β1 can be successfully used to construct cell models (Ji et al., 2018; Wang et al., 2016). Similarly, 1–10 ng/ml TGF-β1 was selected to treat cells in previous studies, and the results showed that 5 ng/ml TGF-β1 can stably and effectively induce cell fibrogenesis, such as cell proliferation, epithelial-mesenchymal transition (EMT), morphologic changes, and high expression of fibrosis-related genes and proteins (Deng et al., 2020; Wang et al., 2021; Wang et al., 2019). Therefore, 5 ng/ml TGF-β1 was used in this study. Cells in complete medium were seeded in 6-well plates for 24 hours at 37°C. After 12 hours of serum starvation, the cells were treated with 5 ng/ml TGF-β1 (HEK293 derived; PeproTech; Rocky Hill, NJ) with or without DR7dA for 1 hour or 48 hours.

MTT Assay. Cells in complete medium were seeded in 96-well plates for 24 hours and treated with DR7dA (0, 10, 20, 40, 80, or 160 μM) without FBS for 24 hours. 3-(4,5-Dimethylthiazol-2-yl)-2,5-diphenyltetrazolium bromide (MTT) (5 mg/ml; Sigma-Aldrich, St. Louis, MO) was added to each well, and the cells were incubated for 4 hours at 37°C. Then, the original medium was removed, and 150 μl of DMSO was added to each well. After gentle shaking, the absorbance was measured at 570 nm. The percent survival is shown as the percentage relative to the control.

ROS Generation Assay. As in previous research (Wang et al., 2019), cells in complete medium were seeded in glass-bottom cell culture dishes for 24 hours at 37°C. After 12 hours of serum starvation, the cells were cultured with 5 ng/ml TGF-β1 alone or with DR7dA for 12 hours. Furthermore, they were incubated in medium containing 2',7'-dichlorodihydrofluorescein diacetate (DCFH-DA, 10 μM; Sigma-Aldrich) for 30 minutes. The ROS signal was captured by confocal microscopy.

Immunofluorescence. Cells in dishes were fixed for 15 minutes at room temperature. The cells were incubated with primary antibodies (in Table 1) overnight at 4°C after being blocked with 10% bovine serum albumin for 1 hour at 37°C. Secondary antibodies were added to label the target proteins, and the cells were incubated for 1 hour at room temperature. The nuclei were stained with 4',6-diamidino-2-phenylindole. Images were acquired with a confocal microscope.

Animals and Treatments. Mice were considered the first-line animal model for preclinical testing (Jenkins et al., 2017), and C57BL/6 mice were consistently prone to BLM-induced PF. Most studies were performed in mice 6–8 weeks old (∼20 years old in humans) (Jenkins et al., 2017; O'Dwyer and Moore, 2018) because aging may directly lead to many age-related respiratory diseases, the most common of which is PF (Birch et al., 2018; Schafer et al., 2017; Selman and Pardo, 2014). Meanwhile, male sex hormones exacerbate PF (Voltz et al., 2008). Therefore, specific pathogen-free female C57BL/6 mice (8 weeks old, 18–22 g) were purchased from the Laboratory Animal Center of Lanzhou University [SCXK(Gan)2018-0002]. All animals underwent 1 week of adaptive feeding before the experiments at 22° ± 2°C.

The BLM-induced PF model is the most commonly used preclinical model *in vivo* because pathologic changes are most similar to human PF (Chua et al., 2005). The BLM-induced animal model is widely used in the assessment of potential antifibrotic agents, and a large number of compounds have been shown to prevent fibrotic progression (Kolb et al., 2020). It has also been reported that intratracheal instillation of 2–5 mg/kg BLM alone can induce PF in C57BL/6 mice (Li et al., 2021). As reported in previous studies, 5 mg/kg BLM can effectively and significantly induce PF, and subcutaneous injection of DR8 and

TABLE 1
Antibody used for Western blot, immunohistochemistry, and immunofluorescence

Antibodies	Species	Western Blot	Immunohistochemistry	Immunofluorescence	Source
α-SMA	Rabbit	1:500	1:200		Abcam
Fibronectin	Rabbit	1:1000			Abcam
Collagen I	Rabbit	1:1000	1:500	1:100	Servicebio
MMP2	Rabbit	1:500			Servicebio
Vimentin	Rabbit	1:1000			Cell Signaling Technology
NOX4	Rabbit	1:200	1:200	1:100	Boster
TGF-β1	Rabbit	1:1000			Abcam
p-ERK	Rabbit	1:1000			Cell Signaling Technology
p-P38	Rabbit	1:1000			Cell Signaling Technology
p-JNK	Rabbit	1:1000			Cell Signaling Technology
ERK	Rabbit	1:1000			Beyotime
P38	Rabbit	1:1000			Cell Signaling Technology
JNK	Rabbit	1:1000			Beyotime
GAPDH	Rabbit	1:5000			Proteintech
HRP-conjugated IgG	Goat	1:10000			ImmunoWay
CoraLite594-conjugated	Goat			1:200	Proteintech

DR8 analogs (0.5 mg/kg/d) showed good antifibrotic activity, low toxicity, and few effects at this dose (Deng et al., 2020; Wang et al., 2021; Wang et al., 2019). Therefore, the same experimental scheme was performed, and 0.5 and 2.5 mg/kg/d were determined as the dosage regimen of DR7dA in this experiment.

Wei et al. believed that the basic number of small animal experiments should be ≥10 in the Methodology of Pharmacological Experiment (Wei et al., 2010). To avoid <10 samples caused by death during the process, ≥11 mice were randomly divided into each group. The mice were randomly divided into six groups: the normal group (n = 11), saline group (n = 11), BLM group (n = 12), DR7dA groups (0.5 and 2.5 mg/kg, n = 11), and N-acetyl-L-cysteine (NAC) group (600 mg/kg, n = 11) (Li et al., 2020). Except in the normal group, saline with 5 mg/kg BLM (Nippon Kayaku; Tokyo, Japan) or saline was injected intratracheally into the mice. The DR7dA groups were subcutaneously injected with 0.5 or 2.5 mg/kg/d, and the NAC group was given 600 mg/kg/d by gavage. An equal amount of saline was subcutaneously injected into the mice in the normal group and the saline group for 21 consecutive days. All mice were euthanized (sodium pentobarbital, 50 mg/kg, intraperitoneal injection), 0.8–1 ml blood was collected from the orbit, and approximately 0.2 ml serum was collected after centrifugation (5000 rpm, 30 min). The whole lung tissues were washed with cold PBS to remove the residual blood. Some of the lung was fixed in 10% formalin solution for 48 hours before paraffin embedding and sectioning, and the remaining tissue was stored at −80°C.

Mouse experiments were approved by the Animal Experiments Committee of the Lanzhou University [SYXK(Gan)2018-0002]. All operations were performed under anesthesia (sodium pentobarbital, 50 mg/kg, intraperitoneal injection), and all efforts were made to minimize suffering.

Tissue Histology and Immunohistochemistry. Hematoxylin and eosin and Masson's trichrome staining were performed on 4-μm sections. The lung sections were deparaffinized and rehydrated. Immunohistochemistry was performed with an SP kit (ZSGB-Bio; Beijing, China). Endogenous peroxidase was blocked after antigen retrieval. After blocking, the sections were incubated with primary antibodies (Table 1) overnight at 4°C. Incubation with a secondary antibody (ZSGB-Bio) was performed at room temperature, and the sections were visualized with 3,3'-diaminobenzidine and hematoxylin. The staining intensity was observed using an optical microscope and analyzed by ImageJ.

Serum Biochemical Measurements. The levels of superoxide dismutase (SOD), malondialdehyde (MDA) and catalase (CAT) in serum were detected using commercial kits according to the instructions (Nanjing Jiancheng Bioengineering Institute; Nanjing, China).

Western Blot Analysis. Proteins were obtained from cells and tissue using radio immunoprecipitation assay lysis buffer (Beyotime; Shanghai, China). The proteins were separated via 10% SDS-PAGE after detecting the protein concentrations with a bicinchoninic acid protein assay kit (Thermo; Rockford, IL) and then transferred to a PVDF membrane (Millipore; Bedford, MA). The membrane was blocked with 6% nonfat dry milk for 1 hour and then incubated with primary antibodies at 4°C overnight. After the bands were incubated with horseradish peroxidase (HRP)-conjugated secondary antibodies for 1 hour, the proteins were visualized with an enhanced chemiluminescence kit (Yeasen Biotech; Shanghai, China). The signals were measured using Evolution Capt software (Vlber Lourmat; Marne la Vallée, France), and glyceraldehyde-3-phosphate dehydrogenase (GAPDH) was used as an internal control. The antibodies are listed in Table 1.

Real-Time Quantitative Polymerase Chain Reaction. TRIzol (Takara; Kusatsu, Japan) was used to extract RNA from cells and tissue. The RNA was reverse transcribed after quantification. Real-time quantitative polymerase chain reaction (RT-qPCR) was used on an Applied Biosystems. The $2^{-\Delta\Delta Ct}$ method with GAPDH as the internal reference was used to quantify the target genes. The sequences are shown in Table 2.

Statistical Analysis. The statistical analyses were performed using GraphPad Prism 8.3.0 (San Diego, California). Each experiment was performed more than three times, and all data are expressed as the mean ± S.D. One-way ANOVA followed by Tukey's post hoc test was used for analyses among groups. $P < 0.05$ was considered to indicate statistical significance.

Results

DR7dA Inhibits TGF-β1–Induced PF *In Vitro*. After purification by RP-HPLC and characterization by mass spectrometry (Supplemental Fig. 1), DR7dA with a purity of 100% (Supplemental Fig. 2) was used in the following experiments. The structure of DR7dA is shown in Fig. 1A; the red part is D-Ala. Then, we compared the stability of DR7dA with that of DR8 (70.19 ± 6.83 min) (Wang et al., 2021) *in vitro* and found that the stability of DR7dA (201.08 ± 58.86 min) was greatly improved in serum. Then, we explored the activity of DR7dA. In PF, both epithelial cells and fibroblasts are involved in the fibrotic process, so A549 and NIH3T3 cells were selected to study the activity of DR7dA *in vitro*. First, to evaluate the cell safety of DR7dA, we used MTT assay to evaluate the toxicity of DR7dA in cells. We used five concentrations of DR7dA ranging from 10 to 160 μM. Unsurprisingly, compared with the control, DR7dA did not show a cytotoxic effect at 160 μM (Fig. 1, B and C). Subsequently, we performed a preliminary study on the activity of DR7dA in two cell lines. TGF-β1 can induce cell proliferation and activation *in vitro*, thus, it is commonly used to establish fibrosis models. Transformation of

TABLE 2
Primer pairs used for RT-qPCR

Gene	Forward primer (5′- 3′)	Reverse primer (5′- 3′)
Human		
ACTA2	ACTGCCTTGGTGTGTGACAA	CACCATCACCCCCTGATGTC
FN1	ACAACACCGAGGTGACTGAGAC	GGACACAACGATGCTTCCTGAG
COL1A1	GTGCGATGACGTGATCTGTGA	CGGTGGTTTCTTGGTCGGT
VIM	AGGCAAAGCAGGAGTCCACTGA	ATCTGGCGTTCCAGGGACTCAT
MMP2	GATACCCCTTTGACGGTAAGGA	CCTTCTCCCAAGGTCCATAGC
NOX4	CTTCCGTTGGTTTGCAGATT	TGGGTCCACAACAGAAAACA
GAPDH	GTCTCCTCTGACTTCAACAGCG	ACCACCCTGTTGCTGTAGCCAA
Mouse		
Acta2	ACTGGGACGACATGGAAAAG	CATCTCCAGAGTCCAGCACA
Fn1	ATGTGGACCCCTCCTGATAGT	GCCCAGTGATTTCAGCAAAGG
Col1a1	GCTCCTCTTAGGGGGCCACT	CCACGTCTCACCATTGGGG
Vim	CGTCCACACGCACCTACAG	GGGGGATGAGGAATAGAGGCT
Mmp2	CAAGTTCCCCGGCGATGTC	TTCTGGTCAAGGTCACCTGTC
Nox4	GAAGGGGGTTAAACACCTCTGC	ATGCTCTGCTTAAACACAATCCT
Sod1	AACCAGTTGTGTTGTCAGGAC	CCACCATGTTTCTTAGAGTGAGG
Sod2	CAGACCTGCCTTACGACTATGG	CTCGGTGGCGTTGAGATTGTT
Cat	AGCGACCAGATGAAGCAGTG	TCCGTGCTCTGTCAAAGTGTG
Tnf	CCCTCACACTCAGATCATCTTCT	GCTACGACGTGGGCTACAG
Il1b	CTGCAGCTGGAGAGTGTGG	GGGGAACTCTGCAGACTCAA
Il-6	AGTTGCCTTCTTGGGACTGA	TCCACGATTTCCCAGAGAAC
Tgfb1	ATGGTGGACCGCAACAAC	CCAAGGTAACGCCAGGAA
Gapdh	AGGAGTAAGAAACCCTGGAC	CTGGGATGGAATTGTGAG

fibroblasts into myofibroblasts is associated with an increase in ECM products, and α-SMA can serve as an indicator of PF. Therefore, TGF-β1–induced cell models were selected in our study, and α-SMA was used for testing in a preliminary study. As expected, α-SMA expression increased in NIH3T3 and A549 cells incubated with TGF-β1. DR7dA suppressed
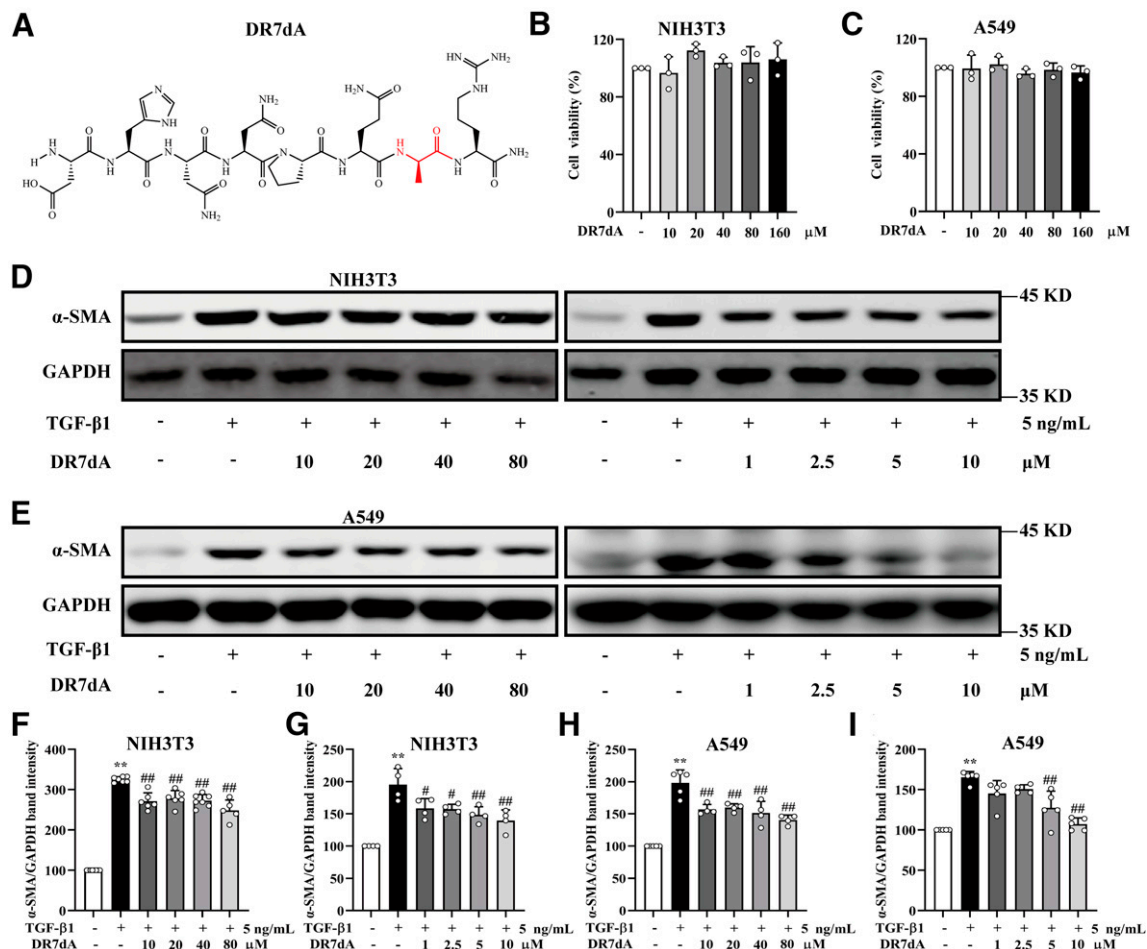

Fig. 1. DR7dA inhibits TGF-β1-induced α-SMA expression *in vitro*. (A) Structure of DR7dA. (B and C) Cytotoxicity of DR7dA in NIH3T3 and A549 cells. Expression of α-SMA with different concentrations of DR7dA in NIH3T3 (D, F, and G) and A549 (E, H, and I) cells. *$P < 0.05$ and **$P < 0.01$ vs. control; #$P < 0.05$ and ##$P < 0.01$ vs. TGF-β1.

α-SMA in a dose-dependent manner, and a significant reduction was observed at 10 μM in NIH3T3 cells (Fig. 1, D and F) and A549 cells (Fig. 1, E and H). Therefore, we used several concentrations lower than 10 μM and found that the lowest effective concentration of DR7dA was 1 μM in NIH3T3 cells (Fig. 1, D and G) and 5 μM in A549 cells (Fig. 1, E and I). Compared with that of DR8, the effective concentration of DR7dA was lower in both cell lines. Later, 2.5 μM and 10 μM were chosen for NIH3T3 cells, and 5 μM and 10 μM were chosen for A549 cells to further analyze the TGF-β1–induced model *in vitro*. Further results in NIH3T3 (Fig. 2, A and B) and A549 (Fig. 2, A and C) cells showed that DR7dA inhibited the expression of fibrosis-related proteins whose expression was induced by TGF-β1 at selected concentrations, including α-SMA, fibronectin, collagen I, and vimentin. In addition, we examined the effect of DR7dA on fibrogenesis at the genetic level. The results showed that DR7dA inhibited the mRNA expression of *Acta2*, *Fn1*, *Col1a1*, *Vim*, and matrix metalloproteinase 2 (*Mmp2*) in NIH3T3 cells (Fig. 2D) and *ACTA2*, *FN1*, *COL1A1*, *VIM*, and *MMP2* in A549 cells (Fig. 2E) after exposure to TGF-β1. Moreover, immunofluorescence showed that TGF-β1 increased collagen I levels, but this effect was suppressed by DR7dA in A549 cells (Fig. 2F). Compared with DR8, DR7dA not only exhibited better stability but also retained its antifibrotic activity at a lower effective concentration *in vitro*. All results indicated that DR7dA exhibited ideal antifibrotic activity against TGF-β1–induced fibrogenesis by inhibiting cell activation and ECM accumulation.

DR7dA Decreases TGF-β1–Induced Oxidative Damage *In Vitro*. OS is an important pathogenic mechanism of PF, and TGF-β1 can induce oxidative damage and antioxidant deficiency in cells. To verify whether DR7dA, like DR8, can inhibit OS caused by TGF-β1–induced ROS production, we used DCFH-DA to examine intracellular ROS levels. DCFH-DA is an oxidation-sensitive probe that can enter cells and eventually interact with intracellular endogenous ROS to generate fluorescence, so ROS levels were detected by measuring fluorescence intensity. The results showed that TGF-β1 treatment elevated ROS levels, but this effect was attenuated by DR7dA (Fig. 3A) in NIH3T3 and A549 cells. In addition, TGF-β1–induced upregulation of NADPH oxidase 4 (NOX4) expression can produce ROS and cause DNA damage and mitochondrial dysfunction, so we also detected the effect of DR7dA on NOX4 expression. As expected, Western blot and RT-qPCR analyses indicated that DR7dA decreased the protein and mRNA levels of NOX4 in NIH3T3 (Fig. 3, B–D) and A549 cells (Fig. 3, G–I). TGF-β1 not only leads to ROS production but also suppresses antioxidant system components, such as SODs and CAT. As shown in Fig. 3E, the mRNA levels of *Sod1*, *Sod2*, and *Cat* were decreased in the TGF-β1 group but increased after treatment with DR7dA in NIH3T3 cells. Moreover, immunofluorescence also showed that DR7dA decreased NOX4 levels in A549 cells (Fig. 3F). The results showed that DR7dA can reduce TGF-β1–induced oxidative damage and restore the antioxidant system, suggesting that DR7dA may block the PF process by inhibiting OS.

DR7dA Blocks the TGF-β1–Induced MAPK Signaling Pathway *In Vitro*. Once TGF-β1 binds with receptors, it can activate the typical Smad pathway and other atypical pathways. The MAPK pathway is involved in the fibrotic process, cell proliferation, and cell differentiation. To determine the signaling pathway involved in the inhibitory effect of DR7dA

in vitro, the levels of phosphorylated MAPK were analyzed. The results showed that the phosphorylation levels of ERK, P38, and JNK were higher after TGF-β1 exposure than the levels in the control group. A significant decrease in the phosphorylation level was observed after treatment with DR7dA for 1 hour in NIH3T3 (Fig. 4, A and B) and A549 cells (Fig. 4, C and D), but there was no difference between the two concentrations. All data showed that DR7dA slowed PF *in vitro* by suppressing the TGF-β1–induced MAPK pathway.

DR7dA Ameliorates BLM-Induced PF *In Vivo*. Subsequently, a BLM-induced PF model was used to verify the effect of DR7dA *in vivo*. NAC, a precursor of glutathione (GSH) that acts as a ROS scavenger, is extensively used as a positive control in animal PF models (Chen et al., 2013; Hamdy et al., 2012; Li et al., 2020; Mizuguchi et al., 2006), so we used NAC as a positive control in mice. In mouse experiments, the doses of DR7dA were 0.5 and 2.5 mg/kg, and the dose of NAC was 600 mg/kg (Li et al., 2020). As shown in Fig. 5, A and B, we observed continued weight gain of the mice in the normal group and initial weight loss followed by weight gain in the remaining groups. The results of hematoxylin and eosin staining suggested that the normal lung structure was severely destroyed, the alveolar wall was thickened, and inflammatory cells were accumulated after BLM stimulation (Fig. 5C). These changes were reversed by DR7dA and NAC. In PF, high expression of α-SMA results in tissue contraction and decreased lung compliance, and MMP2 can activate TGF-β1 to accelerate fibrosis. The α-SMA expression induced by BLM was reversed by DR7dA, as indicated by immunohistochemical staining (Fig. 5, C and D). The assay indicated that the expression of α-SMA, fibronectin, and MMP2 was notably increased in the BLM group but suppressed by DR7dA and NAC (Fig. 5, E and F). In addition, as shown in Fig. 5, G–I, we observed similar results with regard to the effect of DR7dA on the mRNA expression of *Acta2*, *Fn1* and *Mmp2*, after BLM treatment. These data suggested that DR7dA attenuated the development of fibrosis in a dose-dependent manner. Notably, the effect of DR7dA was equivalent to that of NAC at a dose less than 1/100 of the NAC dose.

DR7dA Alleviates BLM-Induced Collagen Deposition *In Vivo*. Overexpression and deposition of collagen are pathologic features of PF. The results of Masson's trichrome staining showed increased amounts of collagen fibers in the BLM treatment group but decreased amounts in the DR7dA and NAC groups (Fig. 6, A and B). In addition, the level of collagen I was measured by immunohistochemistry (Fig. 6, A and C) and Western blot analysis (Fig. 6, E and F). As expected, the levels of collagen I were significantly increased in the BLM-treated group but reduced by DR7dA and NAC treatment. The *Col1a1* levels also showed the same result (Fig. 6D) in mice. These results confirmed that DR7dA was able to reduce collagen accumulation induced by BLM in mice.

DR7dA Modulates BLM-Induced OS and Inflammation. To verify the impact of DR7dA on BLM-induced oxidative damage, the levels of MDA were measured as indicators of oxidative damage, and the activity of SOD and CAT was determined to evaluate antioxidants in serum. As shown in Fig. 7, A–C, after stimulation with BLM, the MDA content markedly increased, and SOD and CAT activity was inhibited. In contrast, administration of DR7dA decreased the MDA content and enhanced SOD and CAT activity. After exposure to BLM, the mRNA levels of *Sod1*, *Sod2*, and *Cat* were markedly
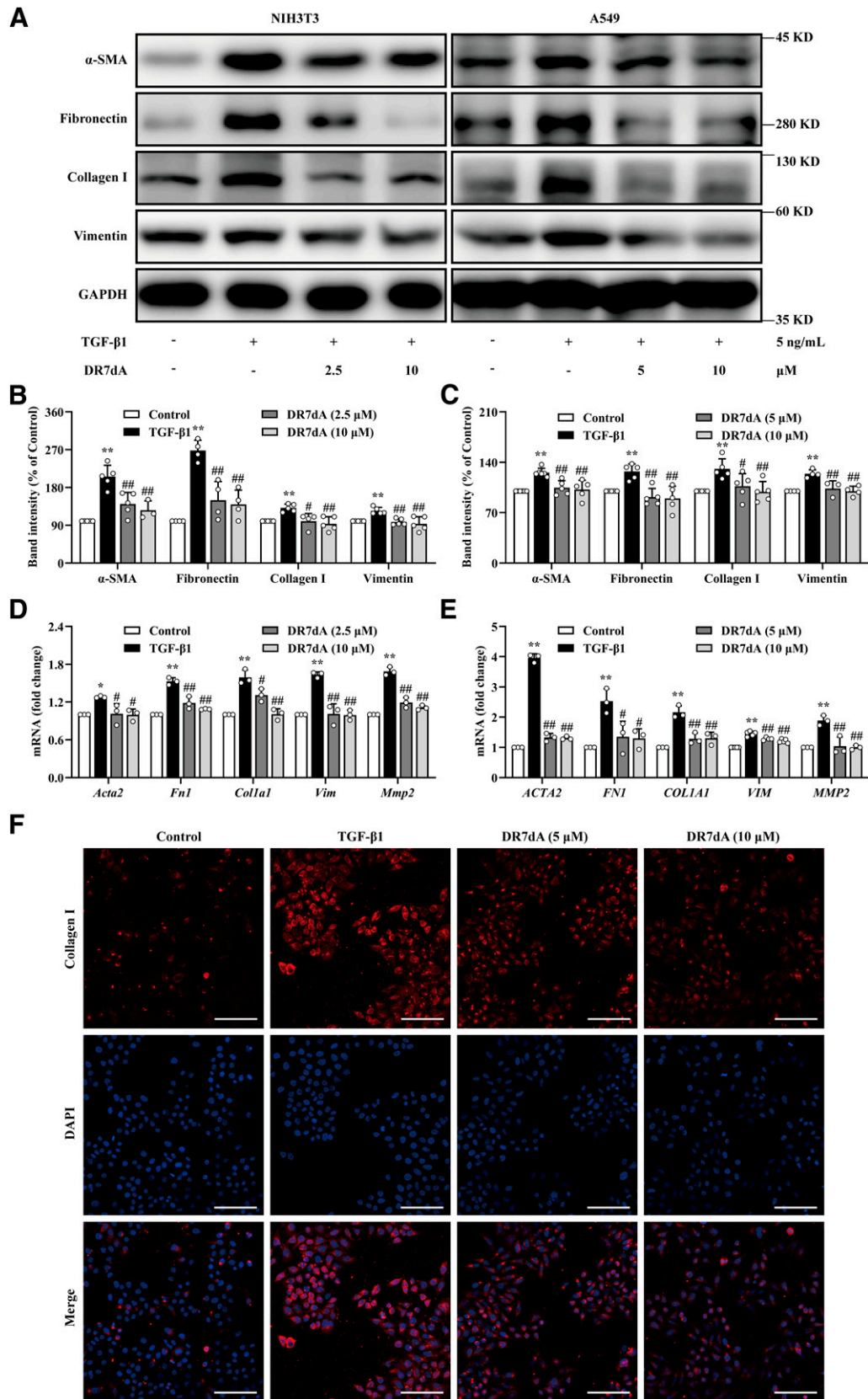
Fig. 2. DR7dA inhibits TGF-β1–induced fibrogenesis *in vitro*. (A) Western blot of α-SMA, fibronectin, collagen I, and vimentin in NIH3T3 and A549 cells. (B) Band quantitative analysis of α-SMA, fibronectin, collagen I, and vimentin in NIH3T3 cells. (C) Band quantitative analysis of α-SMA, Fibronectin, Collagen I, and Vimentin in A549 cells. (D) mRNA levels of *Acta2*, *Fn1*, *Col1a1*, *Vim*, and *Mmp2* in NIH3T3 cells. (E) mRNA levels of *ACTA2*, *FN1*, *COL1A1*, *VIM* and *MMP2*, in A549 cells. (F) Immunofluorescence of collagen I in A549 cells (original magnification, 400×). Scale bars, 100 μm. *$P < 0.05$ and **$P < 0.01$ vs. control; #$P < 0.05$ and ##$P < 0.01$ vs. TGF-β1.
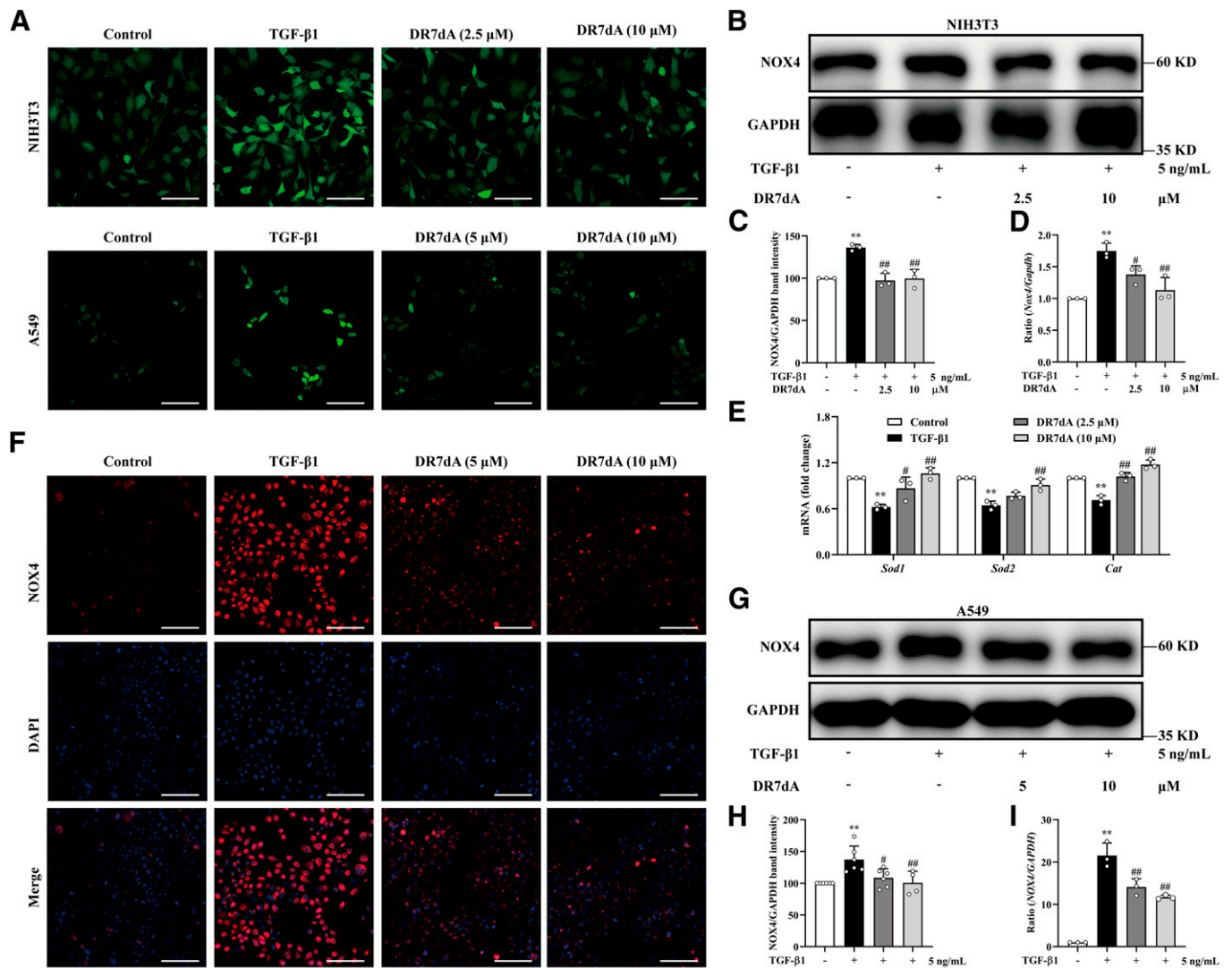
Fig. 3. DR7dA decreases TGF-β1-induced oxidative damage *in vitro*. (A) ROS levels measured with DCFH-DA in NIH3T3 and A549 cells (original magnification, 400×). Scale bars, 100 μm. (B and C) Expression of NOX4 in NIH3T3 cells. (D) *Nox4* mRNA levels in NIH3T3 cells. (E) *Sod1, Sod2,* and *Cat* mRNA levels in NIH3T3 cells. (F) Immunofluorescence staining of NOX4 in A549 cells (original magnification, 400×). Scale bars, 100 μm. (G and H) Level of NOX4 in A549 cells. (I) mRNA expression of *NOX4* in A549 cells. *$P < 0.05$ and **$P < 0.01$ vs. control; #$P < 0.05$ and ##$P < 0.01$ vs. TGF-β1.

lower than those in the control group, but DR7dA recovered the expression of these mRNAs related to antioxidant enzymes (Fig. 7D). Moreover, the changes in NOX4 were measured by RT-qPCR (Fig. 7E) and immunohistochemistry (Fig. 7, F and G). Surprisingly, DR7dA significantly inhibited the BLM-induced increase in NOX4, and the RT-qPCR results showed the same tendency as the immunohistochemistry results regarding the mRNA expression of *Nox4*. Furthermore, tumor necrosis factor (TNF)-α, interleukin (IL)-1β, and IL-6 were elevated in BLM-induced PF and participated in the development of PF. The results showed that the mRNA levels of these inflammatory factors were also reduced by DR7dA (Fig. 7H). These data indicated that DR7dA alleviated PF by restoring the oxidation/antioxidant balance and regulating the inflammatory response in mice in a concentration-dependent manner.

DR7dA Suppresses TGF-β1/MAPK Signaling in BLM-Induced PF. TGF-β1, a major fibrotic cytokine, is considered to regulate various fibrotic processes and is involved in

BLM-induced PF. Unsurprisingly, BLM administration increased TGF-β1 protein and mRNA levels, whereas DR7dA apparently reduced TGF-β1 expression (Fig. 8, A–C). In *in-vitro* studies, we found that DR7dA exerted antifibrotic activity by reducing the TGF-β1–induced phosphorylation of MAPK. We also detected the effect of DR7dA on the MAPK pathway *in vivo*. DR7dA significantly inhibited the BLM-induced increases in the levels of phosphorylated ERK, P38, and JNK (Fig. 8, A and D). These data indicated that DR7dA alleviated BLM-induced PF by regulating the MAPK signaling pathway.

Discussion

Because the lungs are directly connected to the external environment, they are susceptible to the environmental influence. PF is caused by a variety of types of injury to the lung, including poisoning and autoimmune, drug-induced, infectious, and traumatic injuries (Thannickal et al., 2004). Repetitive
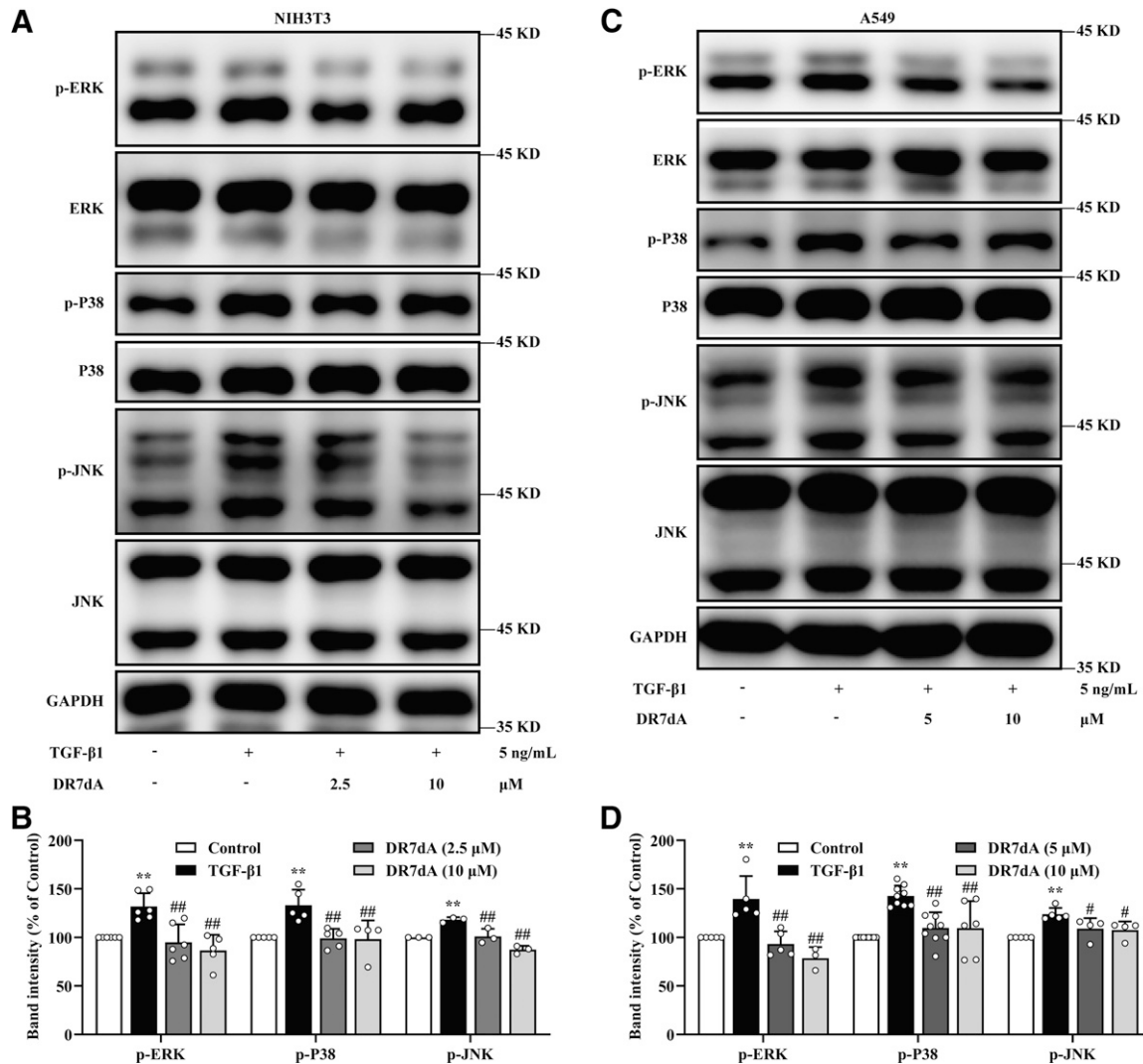
Fig. 4. DR7dA blocks TGF-β1–induced MAPK signaling *in vitro*. (A and B) Levels of ERK, P38, and JNK phosphorylation in NIH3T3 cells. (C and D) Expression of phosphorylated MAPK in A549 cells. *$P < 0.05$ and **$P < 0.01$ vs. control; #$P < 0.05$ and ##$P < 0.01$ vs. TGF-β1.

injury of epithelial cells initiates PF, and alveolar epithelial cells also secrete a variety of profibrotic mediators that induce fibroblast differentiation into myofibroblasts (Sakai and Tager, 2013). Then, fibroblasts proliferate and differentiate into myofibroblasts, producing ECMs. ECM deposition results in alveolar collapse and breathing restriction and eventually leads to respiratory failure and death (Distler et al., 2019; Wynn, 2011). In this study, we found that DR7dA alleviated BLM-induced PF in mice and TGF-β1–induced fibrogenesis in cells. Our results showed that DR7dA inhibited ECM deposition and fibrotic progression *in vitro* and *in vivo*. DR7dA inhibited the differentiation of epithelial and fibroblast cells into myofibroblasts *in vitro* and reduced collagen deposition and pathologic changes *in vivo*.

MMPs can degrade ECM components, but their activity is blocked by tissue inhibitors of MMPs. Many MMPs are involved in fibrosis, such as MMP2, MMP7, MMP9, and MMP28 (Roque et al., 2020). MMP2 is mainly expressed in alveolar epithelial cells in PF, which may be related to basement membrane rupture (Dancer et al., 2011). In our results, DR7dA inhibited BLM-induced elevations in MMP2 protein and mRNA levels *in vivo* and inhibited TGF-β1–induced increases in MMP2

mRNA levels *in vitro*. On the one hand, DR7dA may reduce the damage caused by MMP2 to the basement membrane, which may reduce the invasion of fibroblasts into the alveolar cavity. On the other hand, DR7dA may indirectly inhibit TGF-β1 activation through MMP2, meaning that the activation of TGF-β1–induced downstream signaling is reduced.

After repeated injury, epithelial cells release inflammatory cytokines that recruit inflammatory cells to the site of injury (Wynn, 2011). Innate and adaptive immunity are involved in fibrosis. Neutrophils migrate to damaged tissue under the action of several chemokines and ILs, and macrophages produce TNF-α, IL-1, and IL-6, which maintain tissue inflammation. TNF-α, IL-1, and IL-6 can promote fibrosis in the lungs (Mack, 2018). We found that the increases in *Tnf*, *Il1b*, and *Il6* mRNA levels after BLM stimulation were inhibited by DR7dA, suggesting that DR7dA may inhibit PF through inhibition of inflammation.

Compared with other organs, the lungs are particularly sensitive to OS because they contact higher oxygen levels. At low levels, ROS can mediate normal cellular activities as second messengers. Antioxidants, including CAT, GSH, SOD, and ascorbic acid, exist to clear or remove ROS and prevent OS.
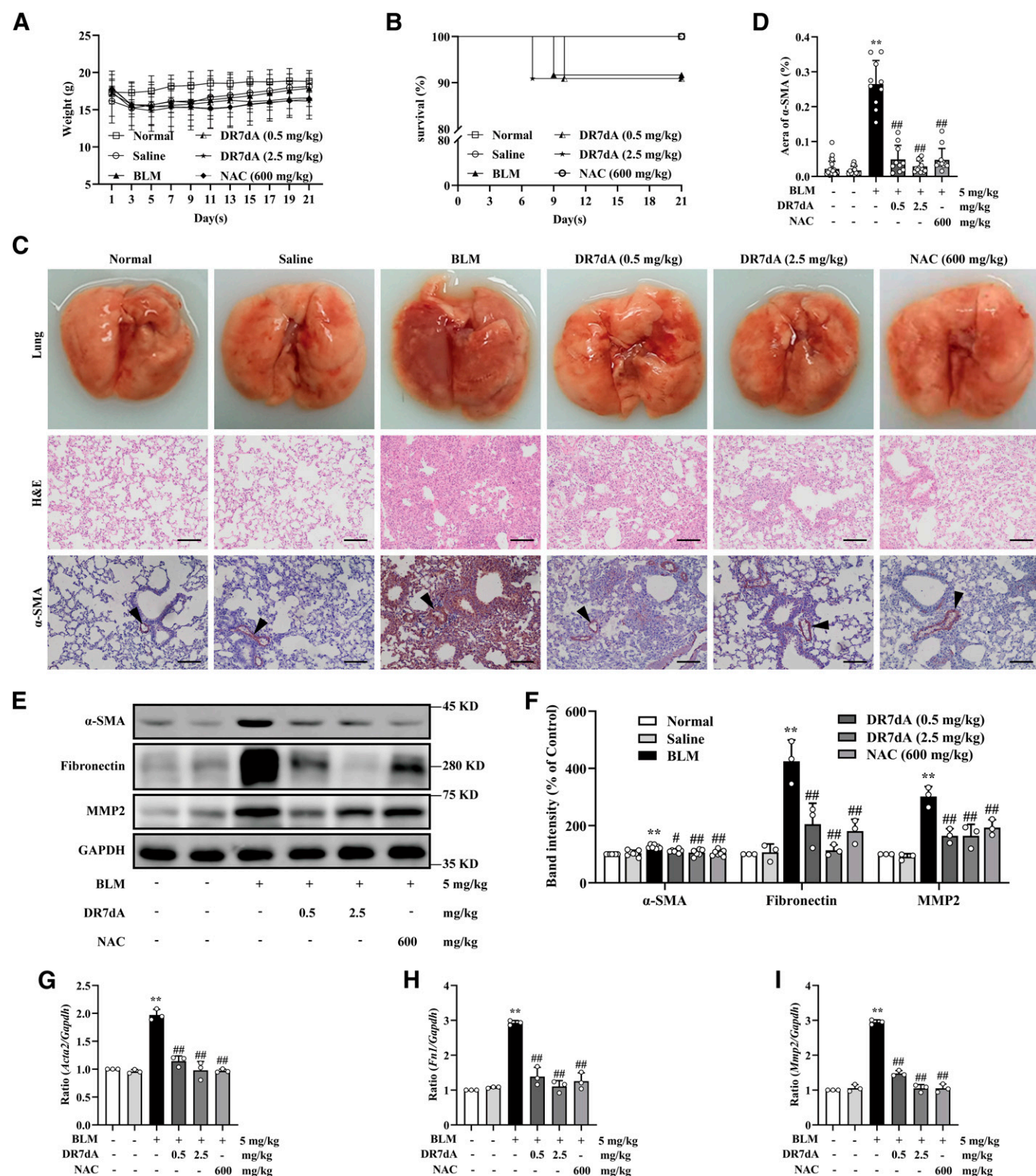
Fig. 5. DR7dA ameliorates BLM-induced PF *in vivo*. (A) Weight changes. (B) Survival. (C) Photos of the lungs, hematoxylin and eosin staining and immunohistochemical staining of α-SMA (original magnification, 100×). Scale bars, 100 μm. (D) Statistical results of immunohistochemical staining. (E and F) Western blot analysis of α-SMA, fibronectin, and MMP2. (G–I) mRNA levels of *Acta2*, *Fn1*, and *Mmp2*. *$P < 0.05$ and **$P < 0.01$ vs. the normal group; #$P < 0.05$ and ##$P < 0.01$ vs. the BLM group.

When the lungs are damaged, excessive ROS can lead to OS, which in turn leads to further ROS production and fibrosis (Kinnula and Crapo, 2003; Kliment and Oury, 2010; van der Vliet et al., 2018). Increases in ROS levels eventually lead to damage to biomolecules, such as proteins, lipids, and DNA, inducing tissue damage and inflammation (Sies and Jones, 2020). In our results, we found that the levels of the lipid peroxidation product MDA were increased, whereas those of the
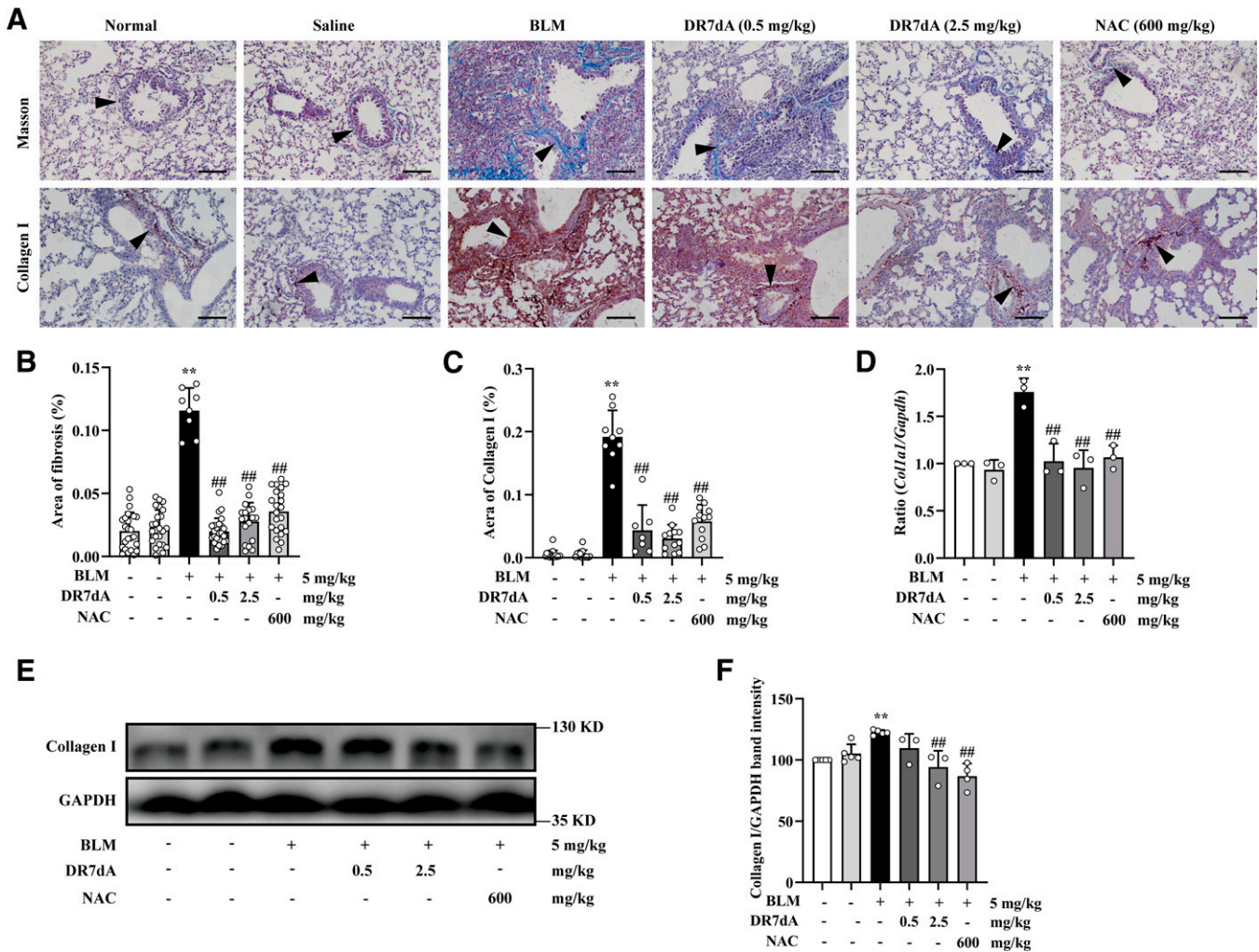
Fig. 6. DR7dA alleviates BLM-induced collagen deposition. (A) Masson's trichrome staining and immunohistochemical staining of Collagen I (original magnification, 100×). Scale bars, 100 μm. (B) Quantitative analysis of Masson's trichrome staining. (C) Quantitative analysis of Collagen I. (D) *Col1a1* mRNA level analyses with RT-qPCR. (E and F) Expression of Collagen I as determined by Western blot analysis. *$P < 0.05$ and **$P < 0.01$ vs. the normal group; #$P < 0.05$ and ##$P < 0.01$ vs. the BLM group.

antioxidant enzymes SOD and CAT were decreased, after BLM induction, indicating the generation of OS. The NOX family is a ROS-generating enzymatic system that plays a role in PF. It has been reported that NOX4 is the cause of ROS accumulation in PF and that NOX4 is upregulated in human and mouse PF models (Crestani et al., 2011). NOX4 has been studied more than other NOXs in PF, and unlike other NOXs, NOX4 activity is mainly regulated by gene expression levels (Crestani et al., 2011; Hecker et al., 2012; Hecker et al., 2009). NOX4 is associated with cell proliferation (Chan et al., 2009) and mediates fibroblast differentiation and proliferation (Amara et al., 2010). Elevated NOX4 expression was also observed in the *in vivo* and *in vitro* models, as has been reported previously. The above phenomena were improved after administration of DR7dA to the models, indicating that DR7dA can partially restore TGF-β1–induced and BLM-induced deficiencies in antioxidant defense.

TGF-β is a powerful profibrotic factor, and its expression is increased during the development of fibrosis in many organs. Mammals expressing three subtypes of TGF-β (TGF-β1-3) also express latent associated protein. PF mainly results

from TGF-β1 stimulation (Ask et al., 2008). TGF-β1 is involved in epithelial cell apoptosis, EMT, epithelial cell migration, fibroblast proliferation and differentiation, and myofibroblast activation (Saito et al., 2018). In our studies, TGF-β1 was overexpressed after BLM induction, but this overexpression was reversed after DR7dA treatment *in vivo*.

Activated TGF-β1 binds with receptors to activate the typical Smad pathway. In addition, TGF-β1 signaling is transmitted through other atypical pathways, and the MAPK pathway and phosphatidylinositol-3-kinase pathway take part in the fibrotic process (Derynck and Zhang, 2003). Our results showed that DR7dA improved PF through the MAPK signaling pathway. MAPK signaling is involved in cell proliferation, cell metabolism, cell migration, and cell differentiation (Lavoie et al., 2020; Newton and Holden, 2006; Shaul and Seger, 2007; Weston and Davis, 2002). Many kinases of MAPK include a redox-sensitive site and are very sensitive to ROS inactivation. Apoptosis signal-regulating kinase-1 is an oxidation-sensitive protein that can activate the JNK and P38 pathways (Tobiume et al., 2001). A vicious cycle exists in which ROS activate JNK and mitochondrial outer membrane protein-dependent ROS production,
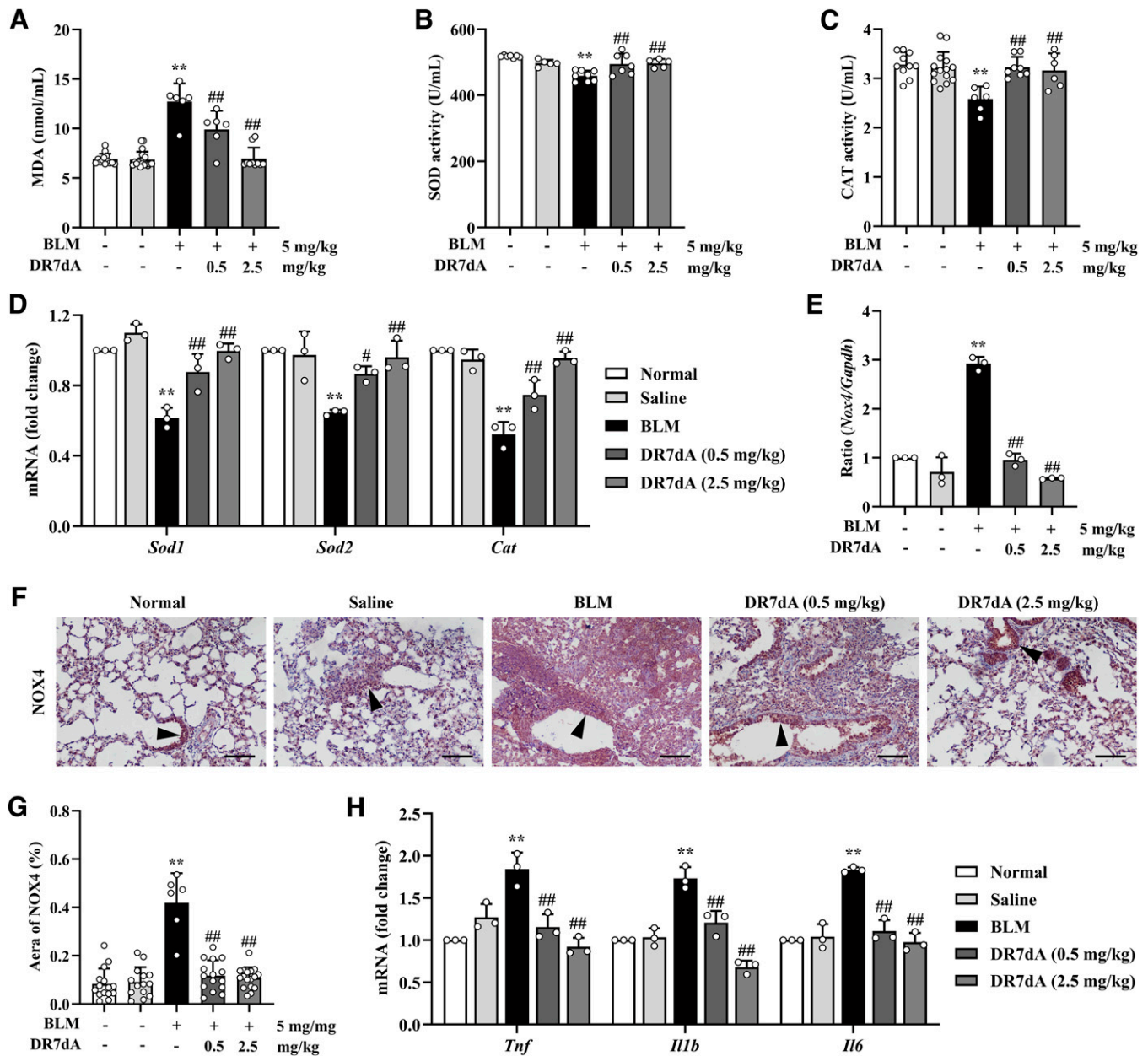
Fig. 7. DR7dA modulates BLM-induced OS and inflammation. (A) MDA content. (B and C) SOD and CAT activity in serum. (D) mRNA expression of *Sod1*, *Sod2*, and *Cat* in mice. (E) RT-qPCR results for *Nox4*. (F) Immunohistochemical staining of NOX4 (original magnification, 100×). Scale bars, 100 μm. (G) Positive staining areas for NOX4. (H) *Tnf*, *Il1b*, and *Il6* mRNA levels measured with RT-qPCR. *$P < 0.05$ and **$P < 0.01$ vs. the normal group; #$P < 0.05$ and ##$P < 0.01$ vs. the BLM group.

resulting in increased ROS production and sustained JNK activation (Blaser et al., 2016; Chambers and LoGrasso, 2011; Win et al., 2014). In our work, DR7dA reduced ROS and NOX4 production, possibly through the JNK and P38 pathways. In addition, P38 plays a major role in adjusting inflammatory expression (Newton and Holden, 2006). Therefore, the inhibitory effect of DR7dA on the inflammatory response may occur through the P38 signaling pathway. However, PF involves complex signaling pathways, and TGF-β1 binds to receptors to activate a variety of pathways; hence, DR7dA may also act through other pathways.

NAC, a precursor of GSH that acts as a ROS scavenger, can effectively reduce BLM-induced PF in mice (Hagiwara et al., 2000). However, in clinical trials, NAC has not been shown to have a beneficial effect on forced vital capacity or mortality (Martinez et al., 2014). On the one hand, blindly eliminating ROS may hinder normal ROS signal transduction, which may aggravate PF. On the other hand, NAC cannot block the source of ROS and may therefore have a limited effect (Gonzalez-Gonzalez et al., 2017; Kato and Hecker, 2020). Therefore, NAC is not recommended for the treatment of PF in clinical practice (even in combination with other drugs) (Cameli et al., 2020). However, because DR8 is an antioxidant peptide, we used NAC as a positive control in our work, and the results showed that NAC can reduce PF, as previously reported. The antioxidative, antiinflammatory,
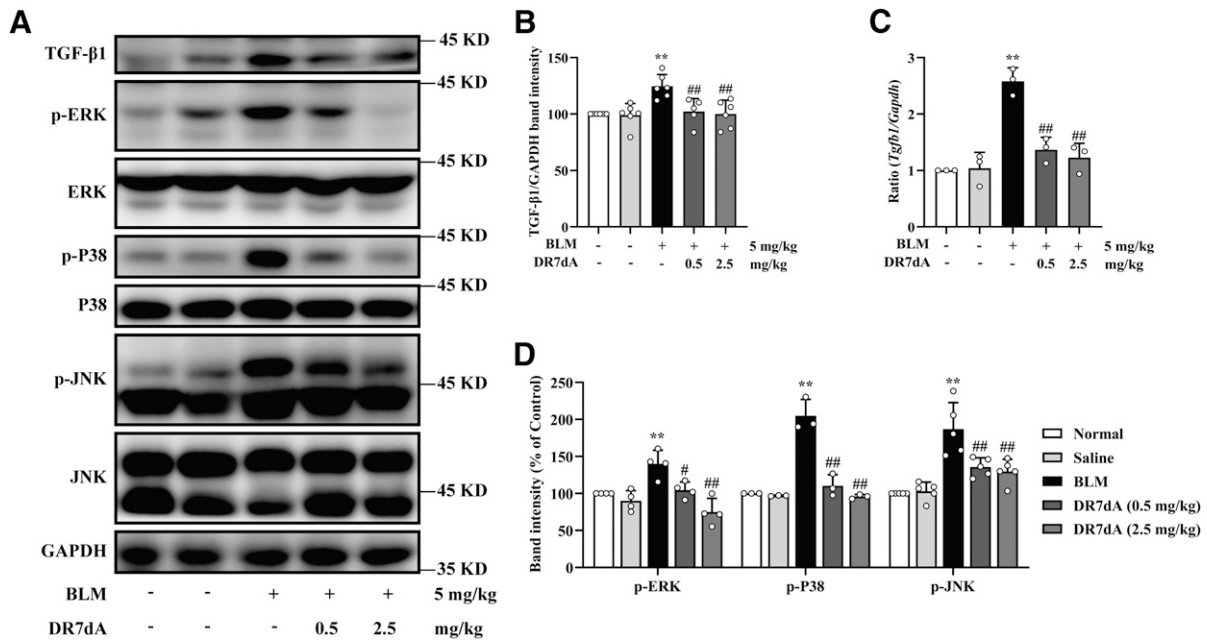
Fig. 8. DR7dA suppresses BLM-induced PF via the TGF-β1/MAPK signaling pathway. (A) Western blot assay of the levels of TGF-β1 and the phosphorylation levels of ERK, P38, and JNK. (B) Statistical result of TGF-β1. (C) The level of *Tgfb1* was measured by RT-qPCR. (D) Band quantitative analysis of the phosphorylation levels of ERK, P38, and JNK. *$P < 0.05$ and **$P < 0.01$ vs. the normal group; #$P < 0.05$ and ##$P < 0.01$ vs. the BLM group.

and antifibrotic effects of DR7dA on PF were equal to or better than those of NAC at a dose of less than 1/100 that of NAC. The administration methods of DR7dA and NAC are different and have also been reported in other literature (Corboz et al., 2018; Guan et al., 2018; Li et al., 2020).

Peptides have the advantages of high activity, low toxicity, and strong specificity, and more peptide drugs are being used in the prevention, diagnosis, and treatment of diseases (Fosgerau and Hoffmann, 2015). However, natural peptides are easily degraded by enzymes *in vivo*, resulting in poor stability and short $t_{1/2}$ values. Long-acting strategies for peptides can extend the $t_{1/2}$ (Erak et al., 2018). Our previous studies have shown that DR8 can reduce BLM-induced PF and unilateral ureteral obstruction-induced renal fibrosis in mice. In this work, the results showed that the serum stability of DR7dA was improved after replacing the Ile of DR8 with D-Ala. DR7dA also showed good antifibrotic activity at a lower effective concentration than DR8. Therefore, the introduction of D-Ala at appropriate sites is a method to optimize active peptides. There is still much work to be done on DR7dA in further studies, such as investigation of the antifibrotic activity of DR7dA in other animal models and evaluation of safety. In addition, different dosing routes and dosages should be tested in animal experiments to determine the best method, and the pharmacokinetics of analogs *in vivo* should be determined to compare the $t_{1/2}$ values *in vivo*.

In summary, after studying the structure-activity relationship through amino acid scanning, we improved the degradation of the natural peptide DR8 *in vivo* by replacing Ile with D-Ala. Compared with DR8, DR7dA not only exhibited better stability but also retained antifibrotic activity in TGF-β1-induced and BLM-induced models. Moreover, we found that the effective concentration of DR7dA *in vitro* was significantly lower than that of DR8. In addition, DR7dA decreased oxidative damage involved in the occurrence and development of PF by inhibiting ROS and NOX4. We have demonstrated that DR7dA

ameliorates PF via the ROS/TGF-β1/MAPK signaling pathway *in vitro* and *in vivo*. Therefore, DR7dA may be a promising candidate compound for the treatment of PF.

Authorship Contributions

Participated in research design: Cheng, Wang, Deng, B. Zhang, Xie.
Conducted experiments: Cheng, Wang, Deng, Li, J. Zhang.
Performed data analysis: Cheng, Guo, Yan, Yue, An.
Wrote or contributed to the writing of the manuscript: Cheng, Wang, Deng, Xie.

References

Amara N, Goven D, Prost F, Muloway R, Crestani B, and Boczkowski J (2010) NOX4/NADPH oxidase expression is increased in pulmonary fibroblasts from patients with idiopathic pulmonary fibrosis and mediates TGFbeta1-induced fibroblast differentiation into myofibroblasts. *Thorax* **65**:733–738.

Ask K, Bonniaud P, Maass K, Eickelberg O, Margetts PJ, Warburton D, Groffen J, Gauldie J, and Kolb M (2008) Progressive pulmonary fibrosis is mediated by TGF-β isoform 1 but not TGF-β3. *Int J Biochem Cell Biol* **40**:484–495.

Birch J, Barnes PJ, and Passos JF (2018) Mitochondria, telomeres and cell senescence: Implications for lung ageing and disease. *Pharmacol Ther* **183**:34–49.

Blanco-Cosa JB and Dawson PE (2008) An efficient Fmoc-SPPS approach for the generation of thioester peptide precursors for use in native chemical ligation. *Angew Chem Int Ed Engl* **47**:6851–6855.

Blaser H, Dostert C, Mak TW, and Brenner D (2016) TNF and ROS crosstalk in inflammation. *Trends Cell Biol* **26**:249–261.

Cameli P, Carleo A, Bergantini L, Landi C, Prasse A, and Bargagli E (2020) Oxidant/antioxidant disequilibrium in idiopathic pulmonary fibrosis pathogenesis. *Inflammation* **43**:1–7.

Chambers JW and LoGrasso PV (2011) Mitochondrial c-Jun N-terminal kinase (JNK) signaling initiates physiological changes resulting in amplification of reactive oxygen species generation. *J Biol Chem* **286**:16052–16062.

Chan EC, Jiang F, Peshavariya HM, and Dusting GJ (2009) Regulation of cell proliferation by NADPH oxidase-mediated signaling: potential roles in tissue repair, regenerative medicine and tissue engineering. *Pharmacol Ther* **122**:97–108.

Chandrudu S, Simerska P, and Toth I (2013) Chemical methods for peptide and protein production. *Molecules* **18**:4373–4388.

Chen Y, Nie YC, Luo YL, Lin F, Zheng YF, Cheng GH, Wu H, Zhang KJ, Su WW, Shen JG, et al. (2013) Protective effects of naringin against paraquat-induced acute lung injury and pulmonary fibrosis in mice. *Food Chem Toxicol* **58**:133–140.

Chua F, Gauldie J, and Laurent GJ (2005) Pulmonary fibrosis: searching for model answers. *Am J Respir Cell Mol Biol* **33**:9–13.

Corboz MR, Zhang J, LaSala D, DiPetrillo K, Li Z, Malinin V, Brower J, Kuehl PJ, Barrett TE, Perkins WR, et al. (2018) Therapeutic administration of inhaled INS1009, a treprostinil prodrug formulation, inhibits bleomycin-induced pulmonary fibrosis in rats. *Pulm Pharmacol Ther* **49**:95–103.

Crestani B, Besnard V, and Boczkowski J (2011) Signalling pathways from NADPH oxidase-4 to idiopathic pulmonary fibrosis. *Int J Biochem Cell Biol* **43**:1086–1089.

Dancer RC, Wood AM, and Thickett DR (2011) Metalloproteinases in idiopathic pulmonary fibrosis. *Eur Respir J* **38**:1461–1467.

Deng B, Yang W, Wang D, Cheng L, Bu L, Rao J, Zhang J, Xie J, and Zhang B (2020) Peptide DR8 suppresses epithelial-to-mesenchymal transition via the TGF-β/MAPK signaling pathway in renal fibrosis. *Life Sci* **261**:118465.

Derynck R and Zhang YE (2003) Smad-dependent and Smad-independent pathways in TGF-beta family signalling. *Nature* **425**:577–584.

Distler JHW, Györfi A-H, Ramanujam M, Whitfield ML, Königshoff M, and Lafyatis R (2019) Shared and distinct mechanisms of fibrosis. *Nat Rev Rheumatol* **15**:705–730.

Erak M, Bellmann-Sickert K, Els-Heindl S, and Beck-Sickinger AG (2018) Peptide chemistry toolbox - transforming natural peptides into peptide therapeutics. *Bioorg Med Chem* **26**:2759–2765.

Fosgerau K and Hoffmann T (2015) Peptide therapeutics: current status and future directions. *Drug Discov Today* **20**:122–128.

Galli JA, Pandya A, Vega-Olivo M, Dass C, Zhao H, and Criner GJ (2017) Pirfenidone and nintedanib for pulmonary fibrosis in clinical practice: Tolerability and adverse drug reactions. *Respirology* **22**:1171–1178.

George PM, Patterson CM, Reed AK, and Thillai M (2019) Lung transplantation for idiopathic pulmonary fibrosis. *Lancet Respir Med* **7**:271–282.

Gonzalez-Gonzalez FJ, Chandel NS, Jain M, and Budinger GRS (2017) Reactive oxygen species as signaling molecules in the development of lung fibrosis. *Transl Res* **190**:61–68.

Guan C, Qiao S, Lv Q, Cao N, Wang K, Dai Y, and Wei Z (2018) Orally administered berberine ameliorates bleomycin-induced pulmonary fibrosis in mice through promoting activation of PPAR-γ and subsequent expression of HGF in colons. *Toxicol Appl Pharmacol* **343**:1–15.

Hagiwara SI, Ishii Y, and Kitamura S (2000) Aerosolized administration of N-acetylcysteine attenuates lung fibrosis induced by bleomycin in mice. *Am J Respir Crit Care Med* **162**:225–231.

Hamdy MA, El-Maraghy SA, and Kortam MA (2012) Modulatory effects of curcumin and green tea extract against experimentally induced pulmonary fibrosis: a comparison with N-acetyl cysteine. *J Biochem Mol Toxicol* **26**:461–468.

Hecker L, Cheng J, and Thannickal VJ (2012) Targeting NOX enzymes in pulmonary fibrosis. *Cell Mol Life Sci* **69**:2365–2371.

Hecker L, Vittal R, Jones T, Jagirdar R, Luckhardt TR, Horowitz JC, Pennathur S, Martinez FJ, and Thannickal VJ (2009) NADPH oxidase-4 mediates myofibroblast activation and fibrogenic responses to lung injury. *Nat Med* **15**:1077–1081.

Hong SY, Oh JE, and Lee KH (1999) Effect of D-amino acid substitution on the stability, the secondary structure, and the activity of membrane-active peptide. *Biochem Pharmacol* **58**:1775–1780.

Jenkins RG, Moore BB, Chambers RC, Eickelberg O, Konigshoff M, Kolb M, Laurent GJ, Nanthakumar CB, Olman MA, Pardo A, et al.; ATS Assembly of Respiratory Cell and Molecular Biology (2017) An official American Thoracic Society workshop report: use of animal models for the preclinical assessment of potential therapies for pulmonary fibrosis. *Am J Respir Cell Mol Biol* **56**:667–679.

Jenssen H and Aspmo SI (2008) Serum stability of peptides. *Methods Mol Biol* **494**:177–186.

Ji YD, Luo ZL, Chen CX, Li B, Gong J, Wang YX, Chen L, Yao SL, and Shang Y (2018) BML-111 suppresses TGF-β1-induced lung fibroblast activation in vitro and decreases experimental pulmonary fibrosis in vivo. *Int J Mol Med* **42**:3083–3092.

Kato K and Hecker L (2020) NADPH oxidases: pathophysiology and therapeutic potential in age-associated pulmonary fibrosis. *Redox Biol* **33**:101541.

Kim JW, Kim TD, Hong BS, Kim OY, Yoon WH, Chae CB, and Gho YS (2010) A serum-stable branched dimeric anti-VEGF peptide blocks tumor growth via anti-angiogenic activity. *Exp Mol Med* **42**:514–523.

Kinnula VL and Crapo JD (2003) Superoxide dismutases in the lung and human lung diseases. *Am J Respir Crit Care Med* **167**:1600–1619.

Kliment CR and Oury TD (2010) Oxidative stress, extracellular matrix targets, and idiopathic pulmonary fibrosis. *Free Radic Biol Med* **49**:707–717.

Kolb P, Upagupta C, Vierhout M, Ayaub E, Bellaye PS, Gauldie J, Shimbori C, Inman M, Ask K, and Kolb MRJ (2020) The importance of interventional timing in the bleomycin model of pulmonary fibrosis. *Eur Respir J* **55**:1901105.

Lavoie H, Gagnon J, and Therrien M (2020) ERK signalling: a master regulator of cell behaviour, life and fate. *Nat Rev Mol Cell Biol* **21**:607–632.

Li C, Sun X, Li A, Mo M, and Zhao Z (2020) S-Allylmercaptocysteine attenuates Bleomycin-induced pulmonary fibrosis in mice via suppressing TGF-β1/Smad and oxidative stress pathways. *Int Immunopharmacol* **79**:106110.

Li S, Shi J, and Tang H (2021) Animal models of drug-induced pulmonary fibrosis: an overview of molecular mechanisms and characteristics. *Cell Biol Toxicol* DOI: 10.1007/s10565-021-09676-z [published ahead of print].

Mack M (2018) Inflammation and fibrosis. *Matrix Biol* **68-69**:106–121.

Martinez FJ, de Andrade JA, Anstrom KJ, King Jr TE, and Raghu G; Idiopathic Pulmonary Fibrosis Clinical Research Network (2014) Randomized trial of acetylcysteine in idiopathic pulmonary fibrosis. *N Engl J Med* **370**:2093–2101.

Mizuguchi S, Takemura S, Minamiyama Y, Kodai S, Tsukioka T, Inoue K, Okada S, and Suehiro S (2006) S-allyl cysteine attenuated CCl4-induced oxidative stress and pulmonary fibrosis in rats. *Biofactors* **26**:81–92.

Newton R and Holden NS (2006) New aspects of p38 mitogen activated protein kinase (MAPK) biology in lung inflammation. *Drug Discov Today Dis Mech* **3**:53–61.

Noto PB, Abbadessa G, Cassone M, Mateo GD, Agelan A, Wade JD, Szabo D, Kocsis B, Nagy K, Rozgonyi F, et al. (2008) Alternative stabilities of a proline-rich antibacterial peptide in vitro and in vivo. *Protein Sci* **17**:1249–1255.

O'Dwyer DN and Moore BB (2018) Animal models of pulmonary fibrosis. *Methods Mol Biol* **1809**:363–378.

Roque W, Boni A, Martinez-Manzano J, and Romero F (2020) A tale of two proteolytic machines: matrix metalloproteinases and the ubiquitin-proteasome system in pulmonary fibrosis. *Int J Mol Sci* **21**:3878.

Saito A, Horie M, and Nagase T (2018) TGF-β signaling in lung health and disease. *Int J Mol Sci* **19**:2460.

Sakai N and Tager AM (2013) Fibrosis of two: epithelial cell-fibroblast interactions in pulmonary fibrosis. *Biochim Biophys Acta* **1832**:911–921.

Schafer MJ, White TA, Iijima K, Haak AJ, Ligresti G, Atkinson EJ, Oberg AL, Birch J, Salmonowicz H, Zhu Y, et al. (2017) Cellular senescence mediates fibrotic pulmonary disease. *Nat Commun* **8**:14532.

Selman M and Pardo A (2014) Revealing the pathogenic and aging-related mechanisms of the enigmatic idiopathic pulmonary fibrosis. an integral model. *Am J Respir Crit Care Med* **189**:1161–1172.

Shaul YD and Seger R (2007) The MEK/ERK cascade: from signaling specificity to diverse functions. *Biochim Biophys Acta* **1773**:1213–1226.

Sies H and Jones DP (2020) Reactive oxygen species (ROS) as pleiotropic physiological signalling agents. *Nat Rev Mol Cell Biol* **21**:363–383.

Thannickal VJ, Toews GB, White ES, Lynch JP III, and Martinez FJ (2004) Mechanisms of pulmonary fibrosis. *Annu Rev Med* **55**:395–417.

Tobiume K, Matsuzawa A, Takahashi T, Nishitoh H, Morita K, Takeda K, Minowa O, Miyazono K, Noda T, and Ichijo H (2001) ASK1 is required for sustained activations of JNK/p38 MAP kinases and apoptosis. *EMBO Rep* **2**:222–228.

van der Vliet A, Janssen-Heininger YMW, and Anathy V (2018) Oxidative stress in chronic lung disease: From mitochondrial dysfunction to dysregulated redox signaling. *Mol Aspects Med* **63**:59–69.

Voltz JW, Card JW, Carey MA, Degraff LM, Ferguson CD, Flake GP, Bonner JC, Korach KS, and Zeldin DC (2008) Male sex hormones exacerbate lung function impairment after bleomycin-induced pulmonary fibrosis. *Am J Respir Cell Mol Biol* **39**:45–52.

Wang D, Cheng L, Li J, Deng B, Yan T, Yue X, Zhang J, Zhang B, and Xie J (2021) Peptide DR8 analogs alleviate pulmonary fibrosis via suppressing TGF-β1 mediated epithelial-mesenchymal transition and ERK1/2 pathway in vivo and in vitro. *Eur J Pharm Sci* **167**:106009.

Wang D, Yan Z, Bu L, An C, Deng B, Zhang J, Rao J, Cheng L, Zhang J, Zhang B, et al. (2019) Protective effect of peptide DR8 on bleomycin-induced pulmonary fibrosis by regulating the TGF-β/MAPK signaling pathway and oxidative stress. *Toxicol Appl Pharmacol* **382**:114703.

Wang X, Ouyang Z, You Q, He S, Meng Q, Hu C, Wu X, Shen Y, Sun Y, Wu X, et al. (2016) Obaculactone protects against bleomycin-induced pulmonary fibrosis in mice. *Toxicol Appl Pharmacol* **303**:21–29.

Wei W, Wu X, and Li Y(2010) *Methodology of Pharmacological Experiment*, 4th ed, People's Sanitary Publishing Press, China.

Werle M and Bernkop-Schnürch A (2006) Strategies to improve plasma half life time of peptide and protein drugs. *Amino Acids* **30**:351–367.

Weston CR and Davis RJ (2002) The JNK signal transduction pathway. *Curr Opin Genet Dev* **12**:14–21.

Win S, Than TA, Fernandez-Checa JC, and Kaplowitz N (2014) JNK interaction with Sab mediates ER stress induced inhibition of mitochondrial respiration and cell death. *Cell Death Dis* **5**:e989.

Wynn TA (2008) Cellular and molecular mechanisms of fibrosis. *J Pathol* **214**:199–210.

Wynn TA (2011) Integrating mechanisms of pulmonary fibrosis. *J Exp Med* **208**:1339–1350.

Address correspondence to: Bangzhi Zhang, School of Basic Medical Sciences, Lanzhou University, 199 Dong Gang West Road, Lanzhou 730000, China. E-mail: zhangbz@lzu.edu.cn; or Junqiu Xie, School of Basic Medical Sciences, Lanzhou University, 199 Dong Gang West Road, Lanzhou 730000, China. E-mail: xiejq@lzu.edu.cn